Graphene-like Dirac states and quantum spin Hall insulators in square-octagonal MX_2 (M = Mo, W; X = S, Se, Te) isomers

Yan Sun,[1] Claudia Felser,[1] and Binghai Yan[1,2,3,4,*]

[1]*Max Planck Institute for Chemical Physics of Solids, 01187 Dresden, Germany*

[2]*Max Planck Institute for the Physics of Complex Systems, 01187 Dresden, Germany*

[3]*School of Physical Science and Technology, ShanghaiTech University, Shanghai 200031, China*

[4]*CAS-Shanghai Science Research Center, Shanghai 201203, China*

(Received 7 May 2015; revised manuscript received 20 August 2015; published 16 October 2015)

We studied the square-octagonal lattice of the transition metal dichalcogenide MX_2 (with M = Mo, W; X = S, Se, and Te), as an isomer of the normal hexagonal compound of MX_2. By band-structure calculations, we observe the graphene-like Dirac band structure in a rectangular lattice of MX_2 with nonsymmorphic space group symmetry. Two bands with van Hove singularity points cross each at the Fermi energy, leading to two Dirac cones that locate at opposite momenta. Spin-orbit coupling can open a gap at these Dirac points, inside which gapless topological edge states exists as the quantum spin Hall (QSH) effect, the 2D topological insulator.

DOI: 10.1103/PhysRevB.92.165421 PACS number(s): 73.20.At, 71.20.−b, 71.70.Ej

Since the discovery of graphene [1,2], research about two-dimensional (2D) materials has been widely explored in both theory and experiment. During the the past few years, transition metal dichalcogenides (TMD) MX_2 (with M = Mo, W and X = S, Se, Te) [3,4] have attracted extensive attention. For example, monolayer of MoS_2 is a direct-gap semiconductor and regarded as massive Dirac systems in the honeycomb lattice with interesting valley physics [5]. Besides, 2D topological insulator (TI) [6,7] phase was also theoretically proposed in MX_2 with $1-T'$ structure [8], and other interesting layered materials such as stanene [9,10] and $ZrTe_5$ [11]. Very recently, an isomer structure of MX_2 in the square-octagonal (so) lattice [12] was found to exhibit gapless band structure with a Dirac cone a the zone center, and lattice distortion [13] was claimed to remove above Dirac cone and induce additional band crossing at the Fermi energy. However, the topological feature in the band structure was neglected due to the missing of spin-orbital coupling (SOC) in calculations. In this work, we revisited the square-octahedral lattices of MX_2 isomers and discovered their graphene-like Dirac band structures (see Fig. 1) and the 2D TI phase. Inspired by the atomic structures of grain boundaries in normal hexagonal MoS_2 [14–16], a square-octagon (so) lattice for MoS_2 [12] was investigated in theory. There are four Mo atoms and eight S atoms in each primitive cell, as shown in Fig. 1. And this lattice can be viewed as repeated square-octagon pairs in both x and y directions. Here, the trigonal prismatic structure of MoS_6 is slightly distorted compared to the hexagonal phase. Furthermore, distortions from the square lattice to a rectangle lattice (distorted-so lattice) were found to optimize the strain in the 2D structure and realize more stable structures [13]. In this work, we adopted the similar lattice structures to TMD MX_2 (with M = Mo and W; X = S, Se, and Te) monolayers and found that the distorted-so lattice is indeed the energetically favored structure for all compounds. The lattice distortion and total energy differences are summarized in Table I. We can see that for lattice distortion, characterized by the ratio of in-plane lattice parameters b/a, becomes stronger as the increasing of atomic radius of atom X for fixed metal atom M, due to the elongated M-X bond.

We mainly focus on their topological electronic properties, after clarifying the lattice structures of MX_2. Our calculations have been performed by using density functional theory (DFT) with projected augmented wave (PAW) method as implemented in the code of Vienna *ab initio* simulation package (VASP) [17,18]. The exchange-correlation energy are considered in the generalized gradient approximation (GGA) level with Perdew-Burke-Ernzerhof (PBE) based density functional [19]. The energy cutoff was set to be 350 eV. The tight binding matrix elements were calculated by projection Bloch states onto maximally localized Wannier functions (MLWFs) [20–22], using the VASP2WANNIER90 interface [23].

Because all the compounds of MX_2 share similar electronic properties, in the following part we will take MoS_2 and WS_2 as the examples for detailed analysis of their electronic structures. Band structures for two types of lattices are compared in Fig. 2. Without the inclusion of SOC effect, band structure in the so lattice presents doubly degenerated d_{z^2} states at Γ point around the Fermi energy for both MoS_2 and WS_2, exhibiting as a semimetallic state. As long as the SOC is taken into consideration, the degenerated d_{z^2} bands split into two single states, with one locating at the top of valence band and the other up shifting to the second conduction band. Beside that, band anticrossing between conduction and valence bands appears around Γ point, which implies the existence of band inversion.

In order to make clear the topological electronic properties, we analyzed the wave functions around the Fermi energy. As presented in Figs. 2(a) and 2(d), the top valence band and bottom conduction bands at Γ point are mainly dominated by $M-d_{z^2}$ and $M-d_{x^2-y^2}$ orbitals, respectively, and these two states have opposite parities. Since two $M-d_{z^2}$ split states are both "−" in parity, the effect of SOC here is just opening the band gap but not changing topological band order. Because of the inversion symmetry in the so lattice, we can directly achieve the topological number of Z_2 invariant by the products of parities at time-reversal invariant momenta (TRIM) [24]. The parity products for occupied states at the three independent TRIMs of Γ(0,0), X((0.5,0),(0,0.5)) and S(0.5,0.5) are "−", "+" and "+", respectively, which gives the Z_2 invariant

*yan@cpfs.mpg.de

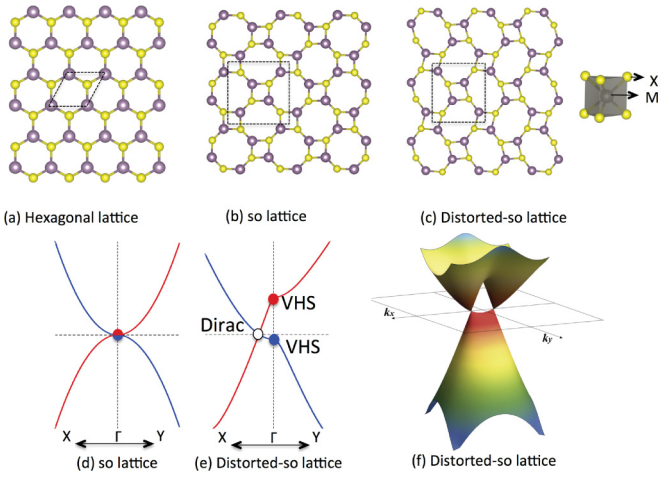

FIG. 1. (Color online) Crystal lattice structure for MX_2 (M = Mo, W; X = S, Se, Te) in the (a) normal hexagonal lattice, (b) square-octagonal (so) lattice, and (c) distorted-so lattice. The primitive unit cell is denoted by dashed lines. The band structures near the Fermi energy are illustrated in the 2D Brillouin zone for (d) so lattice, (e) distorted-so lattice. The 3D plot of the distorted-so lattice is shown in (f), where two Dirac cones forms in the Γ-X line. The Dirac point and the van Hove singularity (VHS) point are indicated by empty and filled circles in (e), respectively.

$\nu_0 = 1$. Therefore, it directly conforms the existence of quantum spin Hall (QSH) insulator state in the so MX_2.

After the lattice distortion, the symmetry decreased from D_{2h} to C_{2h}, and one can expect a dramatically change of the electronic properties. As shown in Figs. 2(b) and 2(e), doubly degenerated M-d_{z^2} states at Γ point split for both MoS_2 and WS_2, even without the inclusion of SOC. Meanwhile, a linear band crossing forms a massless Dirac cone at the Fermi level near Γ point on the line of Γ-X. The crossed two bands are mainly dominated by M-d_{z^2} and M-$d_{x^2-y^2}$ orbitals, respectively. Besides, it is found that the location of the 2D Dirac cone k_D is strongly related to the distortion strength. As given in Table I, the Dirac cone shifts far away from Γ point as the increasing of lattice distortion. With the inclusion of SOC,

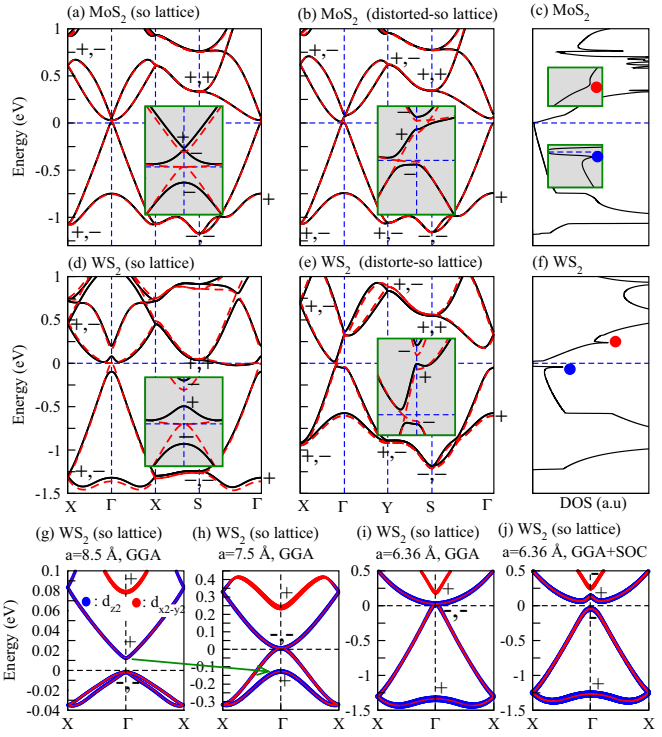

FIG. 2. (Color online) Electronic band structures and density of states (DOS) for MoS_2 and WS_2. Energy dispersion along high symmetry lines in 2D BZ for (a) and (b) MoS_2 with so and distorted-so lattices, and (d) and (e) WS_2 with so and distorted-so lattices. Energy bands with (black solid lines) and without (red dot lines) SOC effect are both included. (c) and (f) are total DOS for distorted-so MoS_2 and WS_2, respectively. DOS are calculated with the inclusion of SOC. Local band structures around Fermi energy are also given in the inserted figures. VHS points in the DOS are remarked with red and blue dots in (c) and (f). (g–j) Evolution of WS_2 bulk band structures as decreasing the lattice constant and inclusion of SOC. The green arrow between (g) and (h) represents that the band inversion occurs between d_{z2} bonding and antibonding states. Band structures are calculated from *ab initio* method, and DOS are calculated from MLWFs. Plus and minus signs are the parity eigenvalues. Fermi energy is set to zero.

TABLE I. The lattice constants and electronic properties of MX_2 (with M = Mo, W; X = S, Se, and Te). Total energy differences between two types of lattices is defined as $\triangle E = E_{\text{so lattice}} - E_{\text{distorted-so lattice}}$ in one primitive cell. In the distorted-so lattice, the linear band crossing at Fermi energy induces a Dirac cone, which locates on the line of Γ−X in the lattice momentum space. Its detailed location (k_D) is defined as the the relative distance away from Γ point, as the schematic diagram given in Fig. 1(b). The *ab initio* calculations for lattice structure optimization, total energy differences $\triangle E$, and location of Dirac cone are preformed without the inclusion of SOC, while for band gap E_g and Z_2 invariants the SOC was included.

	Lattice constant (Å)			E_g (meV)		Z_2 invariant		
	so lattice	Distorted-so lattice	$\triangle E$ (meV)	so lattice	distorted-so lattice	so lattice	distorted-so lattice	k_D ($\frac{2\pi}{a}$)
MoS_2	$a = 6.34$	$a = 6.30, b = 6.37$	0.68	25	12	1	1	0.025
$MoSe_2$	$a = 6.62$	$a = 6.56, b = 6.67$	1.11	38	23	1	1	0.073
$MoTe_2$	$a = 7.06$	$a = 6.72, b = 7.32$	17.87	49	19	1	1	0.201
WS_2	$a = 6.36$	$a = 6.32, b = 6.42$	1.26	111	64	1	1	0.072
WSe_2	$a = 6.64$	$a = 6.30, b = 6.88$	29.50	152	20	1	1	0.225
WTe_2	$a = 7.11$	$a = 6.66, b = 7.37$	87.20	213	19	1	1	0.245

as presented by the local band structures in Figs. 2(b) and 2(e), a general gap is opened with the breaking of the band crossing, which is just a typical image for TIs. Since the distortion does not change the bulk band order, electronic structures are topological equivalent in so lattice and distorted-so lattice. For further confirmation, we also calculated the Z_2 invariant. Though the distortion changes the lattice structure and atomic positions, inversion symmetry is preserved. So parity product at TRIMs is still effective for identifying the topological order [24]. Our calculations found that the Z_2 invariant is 1 for any compound of MX_2, as shown in Table I. Therefore, distorted-so MX_2 is still locating at topological nontrivial state.

The SOC effect becoming stronger along with the increasing of atomic weight, and correspondingly, the SOC opened band gap should be also increased. As given in Table I, it is really the case in so lattice. However, for the distorted-so lattice, the lattice distortion is also becoming stronger as the increasing of atomic radius. Meanwhile, the band crossing point k_D shifts far away from Γ point, as shown in Table I. Hence, the bulk band gap in the situation with distorted-so lattice is decided by a competition between the strengths of SOC and lattice distortion. As presented in Table I, the competed result in this series of compounds gives the largest band gap of about 64 meV, appearance in WS_2.

As we have discussed above, the so lattice and disordered-so lattice have the same band order, and the effect of SOC is just opening the band gap but not inducing band inversion. Therefore, the physics of band inversion can be understood in the so lattice without SOC. We have calculated the band structures with smoothly increasing the lattice constants and found that the band inversion happens between bonding and antibonding d_{z2} states. Taking WS_2 as the example, the evolution of band inversion is given in Figs. 2(g)–2(j), which is similar to the phase transition from CdTe to HgTe [25]. Before the band inversion, the band structure presents as an ordinary band insulator. The top of valence bands are double degenerated W-d_{z2} antibonding state with odd parity, and the bottom of conduction bands is W-d_{z2}-dominated bonding states with even parity. Shrinking the lattice constants, the W-d_{z2} bonding state shifts down to valence bands, as the arrow pointed between Figs. 2(g) and 2(h). And because of the double degeneracy of W-d_{z2} antibonding states at Γ points, the W-$_2$ transforms to semimetallic state along with the band inversion. Going on decreasing the lattice constants, the W-d_{z2} bonding state further shifts down in the energy space, but band order does not change any more. Besides, the W-d_{x2-y2} orbital is closer to the Fermi level and hybridization with W-d_{z2} orbital becomes stronger, as the comparison between Figs. 2(h) and 2(i). However, different from HgTe, the degeneration can be opened by the SOC effect and strain is not necessary here, as presented in Fig. 2(j).

Because of the nontrivial 2D bulk band order in MX_2, topological protected metallic edge state happens. For calculation of the edge state, we have constructed the slab model through MLWFs based tight binding method [20–22]. In so lattice, since the bands around Fermi level are mainly consisted by the hybridized M-d_{z^2} and M-$d_{x^2-y^2}$ orbitals for all the compounds of MX_2, MLWFs are derived from atomic d_{z^2} and $d_{x^2-y^2}$-like orbitals. While for distorted-so lattice, due to the difference between lattice constants of a and b, it is not accurate enough to describe the tight-binding model by only including d_{z^2} and $d_{x^2-y^2}$-like orbitals, in which d_{xy}-like oribtal is also necessary. The tight-binding parameters are determined from the MLWFs overlap matrix. The slab model was constructed in x direction for so lattice due to the cubic symmetry, and both of x and y directions were choose for distorted-so lattice. In order to eliminate the coupling between two edges, the widenesses of the slabs were up to 200 and 100 unit cells for MoS_2 and WS_2, respectively.

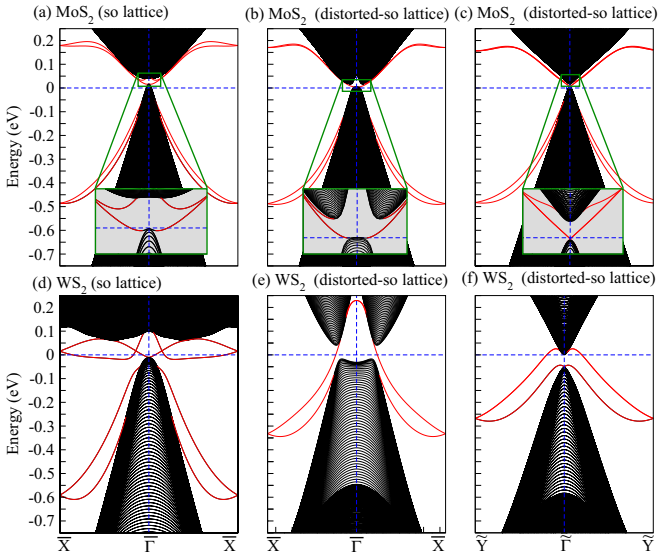

FIG. 3. (Color online) Tight binding edge band structures for (a) so MoS_2, (b) and (c) distorted-so MoS_2 on (0 1) and (1 0) edges, (d) so WS_2, (e) and (f) distorted-so WS_2 on (0 1) and (1 0) edges. Local band structures for MoS_2 around Fermi energy are showing inset. Red curves correspond to edge states. Fermi energy is set to zero.

From Fig. 3 we can see that edge states exist for both so lattice and distorted-so lattice. While the details are depending on different compounds and edge terminations. For example, edge bands cut Fermi level three times for so WS_2, whereas other cases just cut Fermi level once. As the differences of chemical potentials, some cases do not show Dirac pointlike edge states, but the nontrivial Z_2 invariant guarantees the edge bands always cutting Fermi level odd times.

From the DFT band structures we have known that, without inclusion of SOC the so-lattice MX_2 presents as semimetallic state with degenerated M-d_{z^2} locating at Γ point. This degeneration can be regarded as an overlap of two saddle points belonging to the two bands with Van Hove singularity (VHS), as the schematic shows in Fig. 1(d). After lattice distortion, the character of VHS becomes more obvious due to the symmetry breaking. As presented in Fig. 1(e), the two neighboring bands shift upwardly and downwardly, respectively, and the two overlapped saddle points are separated by a band gap around Γ point. The features of VHS are clear in the DFT band structures in Figs. 2(a), 2(b) and 2(d), 2(e), which are further confirmed by the divergence of the density of states (DOS), as presented in Figs. 2(c) and 2(f). Furthermore, as we have seen in the DFT band structures, the lattice distortion also shifts the degenerated point away from Γ point. Similar to graphene,

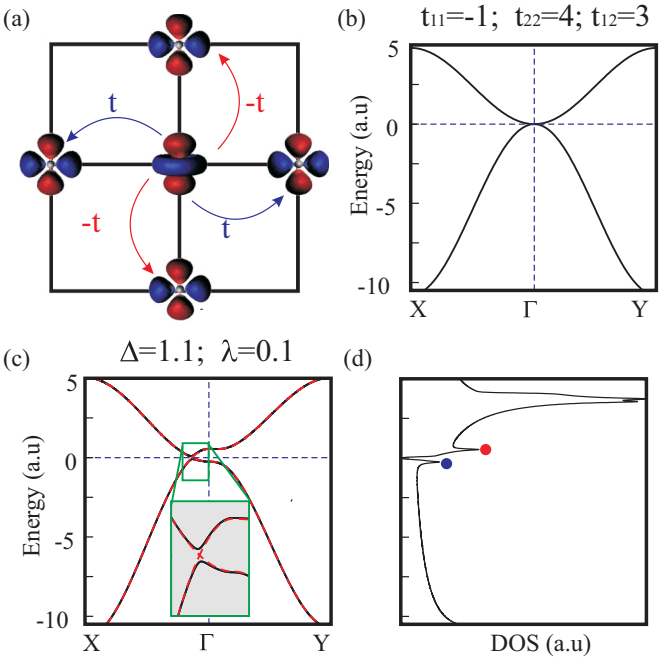

FIG. 4. (Color online) (a) Schematics of the tight-binding model. Two orbitals are illustrated as $d_{x^2-y^2}$ and d_{z^2}. (b) Band structure from the tight-binding model with C_4 rotation symmetry. (c) After breaking C_4 rotation symmetry, the band crossing shifts from Γ point to the high symmetry line between Γ-X. And the band crossing opens with the inclusion of SOC effect. Bands with (black solid lines) and without (red dot lines) SOC effect are both included. (d) Density of states (DOS) corresponding to (c) with the inclusion of SOC. Two peaks related to VHS points are highlighted by red and blue dots.

the new degenerated point exhibits as a massless Dirac cone, and the only difference is the location difference of the Dirac cone in lattice momentum space. In graphene, the Dirac cones paired locate at the high symmetry momentas of K and K', which are connected by inversion and time-reversal symmetry. While in distorted-so MX_2, Dirac cones paired locate at k_D on the line of X-Γ-X, which are also connected by inversion and time reversal symmetry, as shown in Figs. 1(e) and 1(f). SOC is strong enough to open a considerable bang gap in distorted-so MX_2, which is much larger than that of graphene [26]. However, we note that these two VHS bands at the Fermi energy do not induce the topological nature, since both share the same parity.

It is very interesting to explore the physical origin of the Dirac-like states in so MX_2. We project the Wannier Hamiltonian to the wave functions of two VHS bands and derive an effective tight-binding Hamiltonian in a simple square lattice. Although this effective model does not depend on the specific atomic lattice any more, we can still assume a square lattice with two orbitals at one single site. For the sake of simplicity, we take orbitals 1, 2 as $d_{x^2-y^2}$ and d_{z^2}, for example, and the lattice parameter as 1. One can find that the hopping t_{12} between neighboring sites exhibits opposite signs along the x and y directions due to the orbital symmetry, as illustrated in Fig. 4(a). The opposite sign of hopping is the direct cause of VHS bands, which is also revealed in the Wannier Hamiltonian. In the basis of $\{|1\rangle,|2\rangle\}$, the Hamiltonian can be constructed in the nearest hopping approximation,

$$H = (\Delta \cos k_x + \cos k_y - 2)\begin{pmatrix} t_{11} & \\ & t_{22} \end{pmatrix} + (\Delta \cos k_x - \cos k_y)\begin{pmatrix} & t_{12} \\ t_{12} & \end{pmatrix}, \quad (1)$$

where, $t_{i,j}$ ($i,j = 1$ and 2) are the hopping parameters between two nearest orbitals, $\Delta = 1$ corresponds to the square lattice, and $\Delta > 1$ corresponds to a rectangular lattice where the hopping amplitude along x direction is larger than that along y. The "-2" in diagonal terms guarantees that two bands crosses at zero, the Fermi energy, in the square lattice. For the case of square lattice $\Delta = 1$, a kp Hamiltonian can be derived near the Γ point in the form

$$H = -\frac{1}{2}(k_x^2 + k_y^2)\begin{pmatrix} t_{11} & \\ & t_{22} \end{pmatrix} - \frac{1}{2}(k_x^2 - k_y^2)\begin{pmatrix} & t_{12} \\ t_{12} & \end{pmatrix}, \quad (2)$$

where diagonal terms represent two parabolic bands while off-diagonal terms determine the character of a saddle point.

Though SOC matrix elements between atomic orbital $d_{x^2-y^2}$ and d_{z^2} are zeros, the hybridization with other states d_{xy} orbital, as we have seen in the DFT calculations, can induce effective SOC. Therefore, we consider SOC term in a simple way as

$$h_{\mathrm{SOC}} = i\lambda \begin{pmatrix} 0 & 0 & 0 & 1 \\ 0 & 0 & -1 & 0 \\ 0 & 1 & 0 & 0 \\ -1 & 0 & 0 & 0 \end{pmatrix}, \quad (3)$$

with the basis of $\{|1\uparrow\rangle,|2\uparrow\rangle,|1\downarrow\rangle,|2\downarrow\rangle\}$, where λ is the SOC strength. From Fig. 4(c) we can see a band gap opening at the crossing points with the inclusion of SOC effect. Besides, the divergent because of the VHS can also be reproduced in this effective model. As shown in Fig. 4(d), two peaks in the DOS appears due to the saddle point in corresponding band structures. The *ab initio* low-energy bands with VHS and Dirac cones are well reproduced in current tight-binding model.

In conclusion, we have proposed a series of QSH insulators in the isomers of monolayer TMD MX_2 (with M = Mo, W; X = S, Se, and Te) by band structure calculations. The ground-state structures are found to be distorted square-octagonal lattice. Similar to graphene, two bands with Von Hove singularity cross each other and give rise two Dirac cone-like states at the Fermi energy. QSH phases exist when SOC opens an energy gap at the Dirac point. Owing to strong SOC in MX_2, the inverted band gaps are considerable for experiment detection. For example, the band gaps are 12 meV in MoS_2 and 64 meV in WS_2. The QSH phase in MX_2 broadens the physical properties for TMDs, calling for transport and spectroscopy experiments to verify the topological edge states. In addition, the quadratic band touching [27] and Von Hove singularity band with Lifshitz transition in the Fermi surface [28] may promise more exotic phenomena in current systems.

We are grateful to Z. Wang, C.-X. Liu, H. Su, H. Yao, W. Fan, Z.-C. Zhong, and S.-C. Wu for fruitful discussion. We

notice another two works on the similar MoS_2 lattice [29,30] that appeared after our first submission. This work was financially supported by the Deutsche Forschungsgemeinschaft DFG (Project No. EB 518/1-1 of DFG-SPP 1666 "Topological Insulators," and SFB 1143) and by the ERC (Advanced Grant No. 291472 "Idea Heusler").

[1] K. S. Novoselov, A. K. Geim, S. V. Morozov, D. Jiang, Y. Zhang, S. V. Dubonos, I. V. Grigorieva, and A. A. Firsov, Electric field effect in atomically thin carbon films, Science **306**, 666 (2004).

[2] A. H. Castro Neto, F. Guinea, N. M. R. Peres, K. S. Novoselov, and A. K. Geim, The electronic properties of graphene, Rev. Mod. Phys. **81**, 109 (2009).

[3] A. Splendiani, L. Sun, Y. Zhang, T. Li, J. Kim, C.-Y. Chim, G. Galli, and F. Wang, Emerging photoluminescence in monolayer MoS_2, Nano Lett. **10**, 1271 (2010).

[4] K. F. Mak, C. Lee, J. Hone, J. Shan, and T. F. Heinz, Atomically Thin MoS_2: A New Direct-Gap Semiconductor, Phys. Rev. Lett. **105**, 136805 (2010).

[5] D. Xiao, G.-B. Liu, W. Feng, X. Xu, and W. Yao, Coupled Spin and Valley Physics in Monolayers of MoS_2 and Other Group-VI Dichalcogenides, Phys. Rev. Lett. **108**, 196802 (2012).

[6] M. Z. Hasan and C. L. Kane, Colloquium: Topological insulators, Rev. Mod. Phys. **82**, 3045 (2010).

[7] Xiao-Liang Qi and Shou-Cheng Zhang, Topological insulators and superconductors, Rev. Mod. Phys. **83**, 1057 (2011).

[8] X. Qian, J. Liu, L. Fu, and J. Li, Quantum spin Hall effect in two-dimensional transition metal dichalcogenides, Science **346**, 1344 (2014).

[9] Y. Xu, B. Yan, H.-J. Zhang, J. Wang, G. Xu, P. Tang, W. Duan, and S.-C. Zhang, Large-Gap Quantum Spin Hall Insulators in Tin Films, Phys. Rev. Lett. **111**, 136804 (2013).

[10] S.-C. Wu, G. Shan, and B. Yan, Prediction of Near-Room-Temperature Quantum Anomalous Hall Effect on Honeycomb Materials, Phys. Rev. Lett. **113**, 256401 (2014).

[11] H. Weng, X. Dai, and Z. Fang, Transition-metal pentatelluride $ZrTe_5$ and $HfTe_5$: A paradigm for large-gap quantum spin Hall insulators, Phys. Rev. X **4**, 011002 (2014).

[12] Weifeng Li, Meng Guo, Gang Zhang, and Yong-Wei Zhang, Gapless MoS_2 allotrope possessing both massless Dirac and heavy fermions, Phys. Rev. B **89**, 205402 (2014).

[13] H. Terrones and M. Terrones, Electronic and vibrational properties of defective transition metal dichalcogenide Haeckelites: New 2D semimetallic systems, 2D Mater. **1**, 011003 (2014).

[14] S. Najmaei, Z. Liu, W. Zhou, X. Zou, G. Shi, S. Lei, B. I. Yakobson, J.-C. Idrobo, P. M. Ajayan, and J. Lou, Vapour phase growth and grain boundary structure of molybdenum disulphide atomic layers, Nat. Mater. **12**, 754 (2013).

[15] A. M. van der Zande, P. Y. Huang, D. A. Chenet, T. C. Berkelbach, Y. You, G.-H. Lee, T. F. Heinz, D. R. Reichman, D. A. Muller, and J. C. Hone, Grains and grain boundaries in highly crystalline monolayer molybdenum disulphide, Nat. Mater. **12**, 554 (2013).

[16] Z. Zhang, X. Zou, V. H. Crespi, and B. I. Yakobson, Intrinsic magnetism of grain boundaries in two-dimensional metal dichalcogenides, ACS Nano **7**, 10475 (2013).

[17] G. Kresse and J. Hafner, *Ab initio* molecular dynamics for open-shell transition metals, Phys. Rev. B **48**, 13115 (1993).

[18] G. Kresse and J. Furthmiiller, Efficiency of *ab initio* total-energy calculations for metals and semiconductors using a plane-wave basis set, Comput. Mater. Sci. **6**, 15 (1996).

[19] J. P. Perdew, K. Burke, and M. Ernzerho, Generalized Gradient Approximation Made Simple, Phys. Rev. Lett. **77**, 3865 (1996).

[20] N. Marzari and D. Vanderbilt, Maximally localized generalized Wannier functions for composite energy bands, Phys. Rev. B **56**, 12847 (1997).

[21] I. Souza, N. Marzari, and D. Vanderbilt, Maximally localized Wannier functions for entangled energy bands, Phys. Rev. B **65**, 035109 (2001).

[22] A. A. Mostofi, J. R. Yates, Y. S. Lee, I. Souza, D. Vanderbilt, and N. Marzari, wannier90: A tool for obtaining maximally localized Wannier functions, Comput. Phys. Commun. **178**, 685 (2008).

[23] C. Franchini, R. Kovik, M. Marsman, S. S. Murthy, J. He, C. Ederer, and G. Kresse, Maximally localized Wannier functions in $LaMnO_3$ within PBE + U, hybrid functionals, and partially self-consistent GW: An efficient route to construct *ab initio* tight-binding parameters for eg perovskites, J. Phys.: Condens. Matter **24**, 235602 (2012).

[24] Liang Fu and C. L. Kane, Topological insulators with inversion symmetry, Phys. Rev. B **76**, 045302 (2007).

[25] B. Andrei Bernevig, Taylor L. Hughes, and Shou-Cheng Zhang, Quantum spin Hall effect and topological phase transition in HgTe quantum wells, Science **314**, 1757 (2006).

[26] C. L. Kane and E. J. Mele, Quantum Spin Hall Effect in Graphene, Phys. Rev. Lett. **95**, 226801 (2005).

[27] K. Sun, H. Yao, E. Fradkin, and S. A. Kivelson, Topological Insulators and Nematic Phases From Spontaneous Symmetry Breaking in 2D Fermi Systems with a Quadratic Band Crossing, Phys. Rev. Lett. **103**, 046811 (2009).

[28] I. M. Lifshitz, Aomalies of electron characteristics of a metal in the high pressure region, J. Exptl. Theoret. Phys. (U.S.S.R.) **38**, 1569 (1960) [Sov. Phys. JETP **11**, 1130 (1960)].

[29] S. M. Nie, Z. Song, H. Weng, and Z. Fang, Quantum spin Hall effect in two-dimensional transition-metal dichalcogenide haeckelites, Phys. Rev. B **91**, 235434 (2015).

[30] Yandong Ma, Liangzhi Kou, Xiao Li, Ying Dai, Sean C. Smith, and Thomas Heine, Quantum spin Hall effect and topological phase transition in two-dimensional square transition-metal dichalcogenides, Phys. Rev. B **92**, 085427 (2015).